



HAL
open science

Experimental heat flux identification from a braking system

Olivier Quéméner, Frédéric Joly, Alain Neveu

► **To cite this version:**

Olivier Quéméner, Frédéric Joly, Alain Neveu. Experimental heat flux identification from a braking system. *Inverse Problems in Science and Engineering*, 2013, 21 (1), pp.107-128. 10.1080/17415977.2012.672417. hal-01176722

HAL Id: hal-01176722

<https://hal.science/hal-01176722>

Submitted on 25 Aug 2023

HAL is a multi-disciplinary open access archive for the deposit and dissemination of scientific research documents, whether they are published or not. The documents may come from teaching and research institutions in France or abroad, or from public or private research centers.

L'archive ouverte pluridisciplinaire **HAL**, est destinée au dépôt et à la diffusion de documents scientifiques de niveau recherche, publiés ou non, émanant des établissements d'enseignement et de recherche français ou étrangers, des laboratoires publics ou privés.

Experimental heat flux identification from a braking system

Olivier Quéméner*, Frédéric Joly and Alain Neveu

Laboratoire de Mécanique et d'Energétique d'Evry
40 rue du Pelvoux CE1455 Courcouronnes 91020 Evry Cdex FRANCE

This paper presents the Branch Eigenmodes Reduction Method (BERM) applied to the identification of the heat flux dissipated during the friction between a disc rotating at variable speed and two brake pads. Temperature measurements used to identify fluxes in the disc and in the pad come from experimental data. One of the method's strength lies in its ability to greatly reduce the dimension of the numerical problem, while maintaining a satisfying precision on the whole computation domain. The reduction of the model enables to perform the identification in a time compatible with real-time. The identified heat flux is coherent with the mechanical increase due to friction. Small discrepancies observed at the beginning of the friction sequence can be explained by wear.

Keywords: Inverse thermal problem ; Reduced Model ; Branch Modes ; Advection-Diffusion ; experimental braking device

1. Introduction

Due to its vital application in transport, braking process is an active field of research, as evidenced by the rich bibliography (thousands of publications since 1980 ...). As a matter of fact, what seems trivial inside an automobile, reveals to be particularly complex inside a lab : wearing, large plastic deformation, cracking, oxidation of some constituents at the interface of friction ... Given the complex phenomena that occur there, the various existing theoretical models used to predict the thermal behaviour (models with thermal sliding contact resistance and flux sharing coefficient [1], models using a third body of very small thickness placed between both elements in friction [2] [3]), require the knowledge of parameters that can be determined only experimentally. In order to determine those parameters, the heat flux received as sensible heat by each element of the braking system has to be known, as well as their temperature at the interface of friction. The heat flux is identified by inverse method from temperature measurements, and is used to determine the temperature field at the boundary by direct method.

Unfortunately this technique is often unable to be successfully conducted for problems characterized by complex geometries, since it is a mathematically ill-posed problem that requires regularization techniques and the resulting important computing resources (SVD method [4], Tikhonof regularization [5],[6], specification of functions technique [7][8]), limiting applications to 1D or 2D geometries. With the increase of computer resources, standard 3D geometries have been treated recently with the methods presented above [9] [10].

*Corresponding author. Email: o.quemener@iut.univ-evry.fr; tel : +33(0)1 69 47 79 35

Concerning the problem of rotating cylinders involving a transport term in the heat equation, work is less numerous. Chen and Yang [11], using a minimization procedure by conjugate gradients, identified the heat flux at the interface of a roller mill system, for a two-dimensional and stationary configuration. Recently, Yang and Chen [12] identify the heat flux received by a brake disc in a Lagrangian reference frame, which is equivalent to identify a moving source. Non linearities are taken into account. Temperature measurements used in this study are provided by numerical simulation. From experimental results, Volle *et al.* [13] identify the boundary conditions of a rotating cylinder, cooled by the impact of a jet, and heated by an internal heat source. The technique of specification of function is used for a two-dimensional problem, in which the characteristics of the solid on rotation depends on temperature. However, in cases found in the literature, the computational time remains important with those methods.

In order to treat complex 3D geometries, or for a real time identification objective, the size of inverse problems has to be drastically reduced. Different techniques exist: boundary elements method [14], quadrupole formulation [15], non integer identified model [16]. Modal formulations arise naturally in this context. The Modal Identification Method (MIM) is directly based on inverse problems and has been used in many applications : from simple problems, the technique has been gradually improved, and finally enabled to deal with non-linear problems [17] [18]. The Proper Orthogonal Decomposition (POD) is also used for the reduction of inverse problems. In many cases this technique is coupled to a regularization of the problem by Kalman filter [19]. Quemener *et al.* [20] used a Fourier base computed from an eigenvalue problem to identify the flux dissipated at the interface between a fixed pin and a disc rotating at constant velocity, using an experimental bench. Unfortunately, the use of the Fourier base prevents from treating time dependent and non linear problems.

The Branch Eigenmodes Reduction Method (BERM) found in this framework an adequate field for its potentialities, with non-linear three-dimensional applications [21], [22], [23]. Recently the problem of the heat flux received by a disc rotating at variable speed during braking was studied numerically by the authors [24]. It was shown that a new criterion related to the velocity term is added to the one related to the diffusion time. It imposes a very small computation time step, which makes the calculation process particularly long. This problem was solve by BERM on a numerical case, and the authors showed that it was possible to perform this identification in real time by applying a low pass filter on the identified heat flux. To confront this technique to the complexity of a real physical problem, we present here the identification of fluxes dissipated by friction in an experimental braking system. The objective of this study is to prove that BERM is an efficient and fast method to solve inverse problem in industrial configurations, by identifying together the flux received by the disc in rotation and the flux received by the two brake pads.

The article is organized as follows: Sections 2 and 3 describe respectively the experimental device and its modelling. The main elements of the methodology, including modal reduction and the inverse problem formulation, are presented in Section 4. Results are presented and validated in section 5. Finally, section 6 is devoted to the analysis of the physical phenomena.

2. Presentation of the test bench

An automobile braking system is studied, with the whole brake calliper, pads and disc (Fig. 1). For flexibility, the disc is driven by a three phase asynchronous motor via a gearbox limiting the velocity to 150 rpm . A variable speed drive linked to a computer (Fig. 2) enables to impose a time dependent velocity according to a precise sequence, independently of the pressure exerted on the brake. In order to impose the pressure on the disc in rotation, the hydraulic braking system of the vehicle (from the master cylinder to the calliper) is used. A simple system of weights imposes a constant pressure on the master cylinder. The rate of rotation and the electrical power expended by the motor are measured.

Temperature measurement on the rotating disc is made by infrared thermography. The Flir ThermoVision[®] A40 features an uncooled microbolometer detector, and delivers a thermal image composed of 320×240 pixels. Its main limitation is a maximum acquisition frequency of 50 Hz . The relative accuracy of the measurement is estimated to 2%. Since the temperature is measured in the output of the friction zone, it is not possible to apply paint with high emissivity directly on this surface. A groove is machined in the disc (1 mm deep, 2 mm wide) in order to obtain an area which is not in contact with the brake pads. High emissivity paint ($\varepsilon = 0.9$) is apply on the groove as shown in Fig. 1. For reasons of symmetry, this machining is done on both sides of the disc. According to the numerical study of this problem [24], we choose a single measurement point located at $L = 1.5 \text{ cm}$ downstream from the pad (see Fig. 3).

The measurement of temperature in the pads is performed by three inserted thermocouples as shown by Figs. 4 and 5, placed at 6 mm from the friction zone. To check the symmetry of the flux created by the friction, both brake pads are instrumented.

The objective is to identify in real time the heat fluxes dissipated during braking, whose sum has to be compared to the increase of the electric power consumed by the motor. One thus sees that three inverse problems have to be treated simultaneously (Fig. 6) one for the heat flux received by the rotating disc, and two for the heat flux received by both brake pads.

3. Modelling

From the test bench, two models are defined, one for the brake disc and the other one for the brake pads (Fig. 6).

3.1. The brake disc

The considered rotating brake disc is presented in Fig. 3. The disc is made of steel ($k = 49 \text{ W.m}^{-1}.\text{K}^{-1}$, $c = 3.0 \times 10^6 \text{ J.m}^{-3}.\text{K}^{-1}$), has a diameter $D = 26.5 \text{ cm}$ and a thickness $e = 11 \text{ mm}$. Due do its small thickness compared to its transverse dimension and its high diffusivity, the disc is considered two-dimensional. Thermal accommodation phenomena is taking into account on domain Ω_{D1} via $\frac{2h(t)}{e}(T_f - T)$. The disc receives a heat flux on a domain Ω_{D2} from the braking pressure of the brake pads. The heat flux is expressed as a volume power $\Pi(M, t)$ dissipated in the volume Ω_{D2} defined by the contact zone with the brake pads (Fig. 6). The

identification of $\Pi(M, t)$ can be done by two ways. First, the friction zone can be divided in several sub-zones, and the flux is identified, assuming it is uniform in each of them. In the other way, the spatial repartition is supposed of the form :

$$\Pi(M, t) = (A(t) r + B(t) r^2 + \dots)(C(t) \theta + D(t) \theta^2 + \dots) \quad (1)$$

and each parameter is identified. Whatever the chosen method, it is necessary to use several measurement points, judiciously distributed around the friction zone, such as they are actually sensitive to different areas of friction. If this is feasible numerically, it is not the case experimentally. On one hand, an important part of the disc is hidden by the break calliper. On the other hand, multiplying the number of measurement points involve the multiplication of grooves, which limits the friction zone. The simplest physically acceptable solution has been chosen. It is supposed that the energy dissipated is proportional to the velocity, and thus is azimuthally constant and grows linearly with the radius :

$$\Pi(M, t) = \pi(M) f_1(t) = r f_1(t) \quad (2)$$

where $f_1(t)$ is then the temporal evolution to be identified from temperature measurements. This dependency is discussed in paragraph 6.

Expressing velocity as $U(M, t) = \omega(t)U_0(M)$, the physical problem is described by the following equations

$$\begin{aligned} \forall M \in \Omega_{D1} \cup \Omega_{D2}, \\ c \frac{\partial T}{\partial t} = k \nabla^2 T - c \omega(t) \vec{U}_0(M) \cdot \vec{\nabla} T + \frac{2h(t)}{e} (T_f - T) + \pi(M) f_1(t), \end{aligned} \quad (3)$$

with $\pi(M) = 0$ on Ω_{D1} , and $h(t) = 0$ on Ω_{D2} , together with the boundary conditions

$$\forall M \in \Gamma_D, k \vec{\nabla} T \cdot \vec{n} = h(t) (T_f - T). \quad (4)$$

The determination of the heat exchange coefficient is a difficulty. Correlations are found in [25] [26] [27] but for velocities by far greater than those considered in this study. Moreover, depending on the used correlations, results are dispersed. The heat exchange coefficient is then approached by a linear law function of the velocity $\omega(t)$:

$$h(t) = 10 + \beta \omega(t), \quad (5)$$

with $0.13 < \beta < 0.4 \text{ W.m}^{-2} \cdot \text{K}^{-1} \cdot \text{rpm}^{-1}$, yielding a maximum exchange coefficient $30 < h_{max} < 70 \text{ W.m}^{-2} \cdot \text{K}^{-1}$ for a maximum velocity equal to 150 rpm . The influence of parameter β is discussed in paragraph 5.4.

3.2. The brake pad

The pad is composed of a sintered material (Ω_{P1}) and of its support made of steel (Ω_{P2}). Thermophysic parameters of the sintered material have been characterized at the TREFLE lab. (Bordeaux, FRANCE), and were found to be $k = 4 \text{ W.m}^{-1} \cdot \text{K}^{-1}$ and $c = 1.8 \times 10^6 \text{ J.m}^{-3} \cdot \text{K}^{-1}$. The properties of the steel are $k = 50 \text{ W.m}^{-1} \cdot \text{K}^{-1}$ and $c = 3.6 \times 10^6 \text{ J.m}^{-3} \cdot \text{K}^{-1}$. Given the complexity of the geometry (Fig. 4) and the low value of k , a three-dimensional modelling is chosen.

The spatio-temporal evolution of the temperature is modelled by the following equations:

$$\forall M \in \Omega_P, \quad c \frac{\partial T}{\partial t} = k \nabla^2 T, \quad (6)$$

$$\forall M \in \Gamma_{P,i}, \quad i = 1, 3, \quad k \vec{\nabla} T \cdot \vec{n} = h(t)(T_f - T) + \varphi(M)f_2(t). \quad (7)$$

$\Gamma_{p,1}$ is the surface of the pad in friction with the disc. On this boundary, $h(t) = 0$. Similarly to the case of disc, $\varphi(M)$ is the known spatial repartition of the flux, which is assumed to be a linear function of the radius, while $f_2(t)$ is the temporal evolution to be identified from the temperature measurements.

$\Gamma_{p,2}$ is the union of the different surfaces in contact with the ambient air. The top of the pad is placed above the disc and is therefore not in friction and is part of $\Gamma_{p,2}$. Moreover, there is also no friction in the zone facing the groove machined on the disc. On this surfaces, $h(t) = 10 \text{ W.m}^{-2}.\text{K}^{-1}$, and $\varphi(M) = 0$.

A bakelite wafer is added to the back face of the steel support to decrease the thermal losses. On this surface ($\Gamma_{p,3}$), $h = 8 \text{ W.m}^{-2}.\text{K}^{-1}$ and $\varphi(M) = 0$.

4. Methodology

This work is the concrete form of previous theoretical papers. Its objective is to demonstrate the viability of the method in industrial applications. The following paragraph gives the main issues necessary for the global comprehension of this paper. For more details, the reader is encouraged to read the mentioned articles.

4.1. Modal formulation

Combining Eqs. (3)-(7), the general heat equation to solve is :

$$\forall M \in \Omega, \quad c \left(\frac{\partial T}{\partial t} + \omega(t) \vec{U}_0 \cdot \vec{\nabla} T \right) = k \nabla^2 T + a h(t) (T_f - T) + \pi(M) f_1(t), \quad (8)$$

$$\forall M \in \Gamma, \quad k \vec{\nabla} T \cdot \vec{n} = h(t)(T_f - T) + \varphi(M)f_2(t), \quad (9)$$

where a is a numerical parameter whose value is 0 for the pad and $\frac{2}{e}$ for the disc. Modal formulations consist in searching for the solution as a sum of elementary thermal fields V_i , the modes, weighted by their time dependent amplitudes x_i :

$$T(M, t) = \sum_{i=0}^N x_i(t) V_i(M) \quad (10)$$

Rigorously, $N = \infty$, but in practice, only a finite number N of modes is accessible, analytically or numerically. Two issues are raised by Eqs. (8)-(10).

As the heat exchange coefficient $h(t)$ is a function of time, the set of functions V_i has to be able to rebuild boundary conditions (9) for any value of $h(t)$, *i.e.*, it has to form a base for the workspace $H^1(\Omega)$ in order to fulfil the equality in Eq.(10).

Moreover, to be appropriate for on-line identification, the number of unknowns has to be small. A second step is mandatory to reduce the order of the model.

4.2. Branch basis

The eigenfunctions of the branch problem satisfy the boundary condition criteria. This problem is defined by:

$$\forall M \in \Omega, -k\nabla^2 V_i + c\omega_0 \vec{U}_0 \cdot \vec{\nabla} V_i = z_i c V_i, \quad (11)$$

$$\forall M \in \Gamma, k\vec{\nabla} V_i \cdot \vec{n} = -z_i \zeta V_i, \quad (12)$$

where z_i and V_i are, respectively, the eigenvalues and the eigenfunctions of the branch modal base. The specificity of this eigenvalue problem is its boundary condition involving the eigenvalue (Eq. (12)), which means that the branch modal basis defined by Eqs.(11)-(12) is not linked to a specific physical boundary condition. The parameter ζ is a numerical parameter called the Steklov number. It ensures that the eigenvalue z has the same dimension in Eqs. (11) and (12). Its numerical value is chosen in order to balance the integrals on the boundary and on the volume [28]:

$$\zeta = \frac{\int_{\Omega} c \, d\Omega}{\int_{\Gamma} d\Gamma} \quad (13)$$

The introduction of boundary condition (12) leads to two principal kinds of modes [29]. A first family is composed of modes quasi-null on the boundary but not in the bulk of the domain (volume modes), while a second one is made of modes quasi-null on the bulk, but not near the boundaries (surface modes). The existence of surface modes enables to rebuild temperature and thermal flux density for all $h(t)$ convective coefficient. This basis is then adapted to non stationary and non linear thermal problems. Detailed studies of this modes have been performed (see for example [29] or [30]).

4.3. The adjoint branch basis

As this model is non self-adjoint, its eigenmodes do not form an orthogonal set, and the adjoint branch modal base has to be defined :

$$\forall M \in \Omega, -k\nabla^2 V_i^* - c\omega_0 \vec{U}_0 \cdot \vec{\nabla} V_i^* = z_i c V_i^*, \quad (14)$$

$$\forall M \in \Gamma, k\vec{\nabla} V_i^* \cdot \vec{n} = -z_i \zeta V_i^*. \quad (15)$$

The set of functions (V_i, V_i^*) forms a bi-orthogonal system, and verifies the following orthogonality property:

$$\langle \bar{V}_i^*, V_j \rangle = c \int_{\Omega} \bar{V}_i^*(M) V_j(M) d\Omega + \int_{\Gamma} \zeta \bar{V}_i^*(M) V_j(M) d\Gamma = \delta_{ij}. \quad (16)$$

Subscript denotes the order of the eigenmode, $\delta_{i,j} = 1$ if $i = j$ and $\delta_{i,j} = 0$ otherwise, $\langle \cdot, \cdot \rangle$ is the inner product, and \bar{V}_i^* is the complex conjugate of V_i^* .

Evidently, in the case of the brake pad, $\omega = 0$, and the eigenproblem becomes self-adjoint.

The generalized eigenvalue problems Eqs. (11)-(12) and (14)-(15) are defined independently of any spatial discretization. For simple geometries, analytical solution might even be found. However, given the complex geometries, a finite elements discretization with linear shape functions is chosen, leading to a mesh with N_{mesh} nodes. The direct and adjoint branch basis are computed after spatial discretization with the Arpack software [31].

4.4. Reduction

The next step consists in reducing the model, *i.e.* decreasing its size from N to \tilde{N} with $\tilde{N} \ll N$, while keeping the maximum information. This is done by the generalized amalgam method [32]. In this method, the most influential modes are selected, and the remaining modes are added to them, balanced with a coefficient. It ensues new modes \tilde{V}_i , named amalgamated modes, which are expressed as a linear combination of branch modes V_i according to:

$$\tilde{V}_i = \sum_{p=0}^{N_i} \alpha_{i,p} V_{i,p}. \quad (17)$$

The determination of coefficients $\alpha_{i,p}$ is done by minimizing in the modal space the distance between a reference model and the reduced one. The modal decomposition of temperature reads then as:

$$T(M, t) = \sum_{i=0}^{\tilde{N}} \tilde{x}_i(t) \tilde{V}_i(M), \quad (18)$$

4.5. Amplitude equation

The reduced model amplitude equation whose unknowns are \tilde{x}_i , and whose order is \tilde{N} , is obtained by replacing in the variational formulation of Eq. (8)-(9) the temperature field by its modal decomposition (Eq.(18)), while the test functions are the eigenmodes of the adjoint branch problem.

$$\begin{aligned} c \sum_{i=0}^{\tilde{N}} \int_{\Omega} \tilde{V}_j^* \tilde{V}_i d\Omega \frac{\partial \tilde{x}_i}{\partial t} &= -k \sum_{i=0}^{\tilde{N}} \int_{\Omega} \vec{\nabla} \tilde{V}_j^* \vec{\nabla} \tilde{V}_i d\Omega \tilde{x}_i \\ &\quad - c\omega(t) \sum_{i=0}^{\tilde{N}} \int_{\Omega} \tilde{V}_j^* \vec{U}_0 \vec{\nabla} \tilde{V}_i d\Omega \tilde{x}_i \\ &\quad - h(t) \left(a \sum_{i=0}^{\tilde{N}} \int_{\Omega} \tilde{V}_j^* \tilde{V}_i d\Omega \tilde{x}_i + \sum_{i=0}^{\tilde{N}} \int_{\Gamma} \tilde{V}_j^* \tilde{V}_i d\Gamma \tilde{x}_i \right) \\ &\quad + h(t) \left(a \int_{\Omega} \tilde{V}_j^* T_f d\Omega + \int_{\Gamma} \tilde{V}_j^* T_f d\Gamma \right) \\ &\quad + f_1(t) \int_{\Omega} \tilde{V}_j^* \pi(M) d\Omega + f_2(t) \int_{\Gamma} \tilde{V}_j^* \varphi(M) d\Gamma. \end{aligned} \quad (19)$$

$f_1(t)$ and $f_2(t)$ will be identified with this equation from the knowledge of T . Numerical implementation details are given in appendix A.

4.6. Inverse problem

As the objective is to perform on-line identification, the inverse method has to be sequential, which discards global minimization methods such that conjugate gradients. A Beck time-stepping method adapted to the modal formulation has been chosen for both domains (pad and disc). The reduced formulation broadens the scope of investigation of the method of Beck with problems of large dimensions while keeping acceptable computation time. The general formulation of the method used is given in appendix B.

5. Application

5.1. Numerical parameters

The choice of parameters (reduced model order, time step and the number of future time steps) is delicate, since they are linked. The optimum is then obtained from an equilibrium and a sensitivity analysis is required. However, as a reduced model is used, the sensitivity analysis is performed in a short time. For the disc, a complete numerical study, including stability analysis and sensitivity to measurement and material property errors has been conducted by Quéméner *et al.* [24]. For the pad, similar configurations has been fully studied in refs. [22], [23]. The numerical parameters of the reduced models used for the identification process are the following.

The disc is discretized on a mesh containing 4914 nodes. In accordance with [30], the base branch is computed with a low angular velocity $\omega_0 = 0.018 \text{ rpm}$, a conductivity $k = 49 \text{ W.m}^{-1}.\text{K}^{-1}$, volume thermal capacity $c = 3.0 \times 10^6 \text{ J.m}^{-3}.\text{K}^{-1}$, and a Steklov number $\zeta = 2.0 \times 10^5 \text{ J.m}^{-2}.\text{K}^{-1}$. An initial base of 615 modes is computed, reduced to 54 modes with the amalgam procedure. The number of future time steps is equal to 0. The necessary time step is 2.10^{-3} s . The camera frequency being of 50 Hz , temperature records are oversampled using a quadratic law.

The pad is discretized on a mesh containing 6956 nodes. The base branch is computed with a conductivity $k = 4 \text{ W.m}^{-1}.\text{K}^{-1}$, volume thermal capacity $c = 1.6 \times 10^6 \text{ J.m}^{-3}.\text{K}^{-1}$, and a Steklov number $\zeta = 1.3 \times 10^4 \text{ J.m}^{-2}.\text{K}^{-1}$. An initial base of 600 modes is computed, reduced to 50 modes with the amalgam procedure. The number of future time steps is equal to 10, the time step is 0.2 s .

5.2. Experimental mechanical solicitations

The temporal evolution of the disc velocity is shown in Fig. 7. The velocity is linear by segments, varying from 0 to 150 rpm, alternating phases of acceleration, deceleration, constant speed and letup. In order not to have too much torque at low speed (which locks the engine), the pressure on the braking system is imposed only when the disc velocity reached the constant speed steps. Figure 7 also represents the evolution of mechanical power dissipated during the friction known within an uncertainty of 5%. This value is obtained from the difference of electrical power with and without friction, the uncertainty being estimated with the losses by joules effect on the stator engine.

5.3. Validation of the inversion procedure

The heat fluxes dissipated by the pads and by the disc are identified from the temperatures evolution (Fig. 8).

Although the level of temperature is similar, an asymmetry appears clearly between the two pads, the temperature variations in pad n^02 being slower than those observed in pad n^01 , showing the necessity to treat both pads. The identified fluxes for both pads are presented in Fig. 9. Accordingly to the temperature measurements, the flux asymmetry between the two pads is recovered. These heat fluxes are used as input in the direct model (Eq. (19)). Figure 10 compares the temperature evolutions obtained numerically with the experimental ones. The global shape is similar, although discrepancies of a few degrees are observed. Nevertheless, the maximum difference is less than 5%, validating the on-line inversion procedure.

Concerning the temperature at the surface of the disc (Fig. 8), regular oscillations, functions of the speed, appear since the beginning of the heating. These oscillations are in agreement with several studies reported in the literature [33], [34], [35]. They are caused by the existence of hot spot engendered by mechanical phenomena (non uniform wear, contact asperity, thermo-elastic deformations, imperfect geometry of the disc). After the letup of the disc velocity ($t = 240$ s), the amplitude of the temperature oscillations lightly increases then decreases to its initial level.

The identified heat flux dissipated in the disc, presented by Figure 11 for $\beta = 0.27 W.m^{-2}.K^{-1}.rpm^{-1}$, *i.e.* $h_{max} = 50 W.m^{-2}.K^{-1}$, is strongly noised, especially at high velocities. Following the numerical study [24], the raw identified heat flux is filtered with a low pass filter, with a cut-off frequency of $0.3 Hz$ (see Fig. 12). It is remarkable that the raw identified heat flux yields such result after a simple filtering : from a signal varying from $[-10^6 : 10^6] W.m^{-2}$, the filtering gives results in the range $[0 : 1400] W.m^{-2}$. Moreover, this heat flux is consistent with the friction sequence : A stiff increase of the heat flux is observed when a pressure is exerted on the brake, while a stiff decrease is seen when the pressure stops.

The existence of strong oscillations is mainly due to the filter : the low cut-off frequency, imposed by the velocity, limits the number of sinusoids kept to rebuild the signal after the filtering.

The smoothed value of the filtered identified heat flux (see Fig. 12) is chosen as input in the direct simulation. Figure 13 compares the experimental temperature evolution with the numerical one. As expected, the numerical model can not reproduce temperature oscillations, as their causes are not taken into account by the model. However, numerical simulation reproduces faithfully the mean experimental evolution. It is remarked that the numerical model predicts small temperature oscillations during the second stage of acceleration after the suspension of rotation. These oscillations, due to a hot spot engendered by the velocity variation, coincide with lightly larger experimental oscillations. This good agreement validates the inversion procedure for the disc.

5.4. Validation of the inversion results

As stated in section 3.1, an uncertainty for the identification of the heat flux dissipated by the disc comes from the insufficient knowledge of the heat exchange coefficient and its dependency towards the disc velocity. The heat flux is identified

with the extreme values of β (Fig. 15). As expected, the identified heat flux is sensitive to the value of the exchange coefficient, except at the beginning of the experiment, where the disc temperature is close to the ambient, limiting the heat exchange. These fluxes are taken as input for the direct model. Whatever the value of β , the temperature computed with the direct model fits the experiment. As a matter of fact, comparison between experimental and numerical temperatures obtained with the identified flux is only a way to verify the coherency between direct and inverse models. It enables to validate the inversion procedure, but does not enable to validate the identification result. The use of incorrect parameters will yield an incorrect flux, which will yield, with the same wrong parameters, the measured temperature. The insufficient knowledge of h leads to an area of uncertainty (shaded area in figure Fig. 15), for which the maximum value is 8%.

In order to validate the identification results, two complementary ways are used. The heat fluxes received by the three components are first added and compared to the increase of mechanical power due to friction (Fig. 16). Following the first law of thermodynamics, the global heat flux is of the same magnitude than the increase of mechanical power.

Furthermore, the repartition of the global heat flux is compared to the model of semi-infinite solids giving the fraction γ of frictional heat flux entering the disc [36] :

$$\gamma = \frac{\epsilon}{1 + \epsilon} \quad \text{with} \quad \epsilon = \frac{\sqrt{\lambda_D c_D}}{\sqrt{\lambda_P c_P}} \quad (20)$$

With the thermophysical parameters used in this study, $\gamma = 82\%$. By comparing the identified fluxes in the pad and in the disc, it is seen that about 85% of the mechanical power is absorbed by the disc. These two results validate the identification results.

Computations are conducted on a PC cadenced at 1.8 *Ghz* and a memory of 2 *Go* (RAM). With this common hardware, the sequential identification process and the filtering take less than 205 *s* (194 *s* for the disc and 5 *s* for one pad) while the total process duration is 448 *s*. This study proved that identification with BERM is a suitable method for real experimental problems with rotating device, and it opens the way to real-time process.

6. Discussion

At some special moments, especially during the first heating phase, a significant difference appears between the two powers. The question is whether it is an identification error or a physical phenomenon not taken into account in the thermodynamics balance. It is noted that during the second stage of friction, the two fluxes are equal in the limit of the uncertainties. This eliminates systematic errors of modelling such as wrong thermophysical properties or inappropriate two-dimensional simplification.

The examination of Fig. 8 reveals an asymmetry inside both pads, the sensor located downstream measuring a temperature lower than the central and upstream sensor. This is confirmed by the observation of the pad after some experiments (photo 17). It is first seen that some parts of the surface (zone A) have a glossy appearance. This corresponds to the abrasion of the metal grains present in the

sintered materials. The areas of non-friction, especially the part of the pad facing the groove machined into the disc, appear (zone B). Surprisingly, the bottom of the pad (zone C), supposed to be in contact with the disc, does not have the same glossy appearance than zone A. We finally note the existence of a deposit of powder (zone D), coming from the wear of the pad and which is interposed between the pad and disc. These observations also correspond to those found in the rich bibliography insisting on the complexity of the phenomena that occur at the interface between a disc and a plate brake, and which are little known. Furthermore, this non-uniformities of the surface appearance varies according to experimental tests.

The difference of temperature inside pad as well as the examination of the pad prove the complex azimuthal and radial non-uniformity of the flux dissipated at the interface, which is not taken into account in the numerical model. Moreover, given the complexity of the physics and the variation of the solicitations, the spatial repartition of the flux is probably time dependent, explaining the non systematic errors. Radial linear law used in our model is a coarse approximation of reality, and the inclusion of an accurate repartition of the flux in the numerical model might improve the identification results. If the numerical implementation of a sophisticated law is not a fundamental difficulty, it is not the case of its procurement, representative of every phenomenon. A first refinement can be done with a mechanical simulation taking into account the entire braking system, the repartition of the pressure exerted by the master cylinder on the pads and the static jamming. However, the non-uniform wear and the resulting release of particles trapped at the interface between the disc and the pad [37] [38] [39] as well as the dynamic jamming and unjamming are hardly precisely predictable.

The pad wear does not just impact on the heat flux repartition. It also impacts on the thermodynamics budget. A prominent phenomenon is the release of particles from the pad, but also from the disc, which are trapped at the interface. The softer parts are slowly being crushed, and are either expelled or incorporated at the interface in order to form a third body between the two initial bodies. There are also very hard parts, which retain their original size and attack the surfaces of bodies in contact. With the models used here, only the heat flux received by the elements as sensible heat is identified, while there is little doubt that wear occurs without energy supply.

7. Conclusion

The objective of this study was to prove that Branch Eigenmodes Reduction Method (BERM) is an efficient and fast method to solve inverse problem in industrial configurations. The chosen application is the identification of the heat flux dissipated during friction between a rotating disc and two brake pads. The experimental device being close to a real configuration, the identification process is characterized by every bias linked to experimental domain : measurement uncertainties and distortion between the model and its necessary approximations on one hand, and the reality and its complexity on the other hand. BERM depends solely on a mathematical model. To model accurately the reality, thermo-physical parameters (capacity, conductivity, heat exchange coefficient, spatial repartition of the flux...) have to be accurately known. This is the main limitation of our method. However, since they are known, whatever their complexity (time dependency, spatial repartition, non linearity), they can be incorporated in the model. Despite

this limit, this study achieved its objective, as the identification results presented here are in good agreement with the measured mechanical power. Moreover, as the computation time is far below the process duration, it opens the way to real time identification.

This study was confronted to the complex phenomena due to wear. It impacts on the spatial repartition of the heat flux and on the thermodynamics budget, and might explain the small discrepancy observed at the beginning of the experiment. This highlights how the weakness of the method might become a strength: as we know precisely the nature of what is identified, this method, coupled with a sophisticated experimental device used to determine the spatial distribution of the flux, can be a tool to quantify the energetic phenomena involved during the braking process.

References

- [1] N. Laraqi, A. Bairi, and L. Ségui, *Temperature and Thermal Resistance in Frictional Devices*, App. Thermal Engineering 24 (2004), pp. 2567–2581.
- [2] D. Majcherczak, P. Dufrenoy, and Y. Berthier, *Thermal and mechanical coupling aspects of the dry sliding contact*, Tribology International 40 (2006), pp. 834–843.
- [3] A.L. Cristol-Bulthé, Y. Desplanques, and G. Degallaix, *Coupling between friction physical mechanisms and transient thermal phenomena involved in pad-disc contact railway braking*, Wear 263 (2007), pp. 1230–1242.
- [4] J.A.M. García, J.M.G. Cabeza, and A.C. Rodriguez, *Two-dimensional non-linear inverse heat conduction problem based on the singular value decomposition*, Int. J. Thermal Sci. 48 (2009), pp. 1081–1093.
- [5] A. Thikhonov and V. Arsenin *Solutions of ill-posed problems*, V.H. Winston and Sons, Washington D.C., 1977.
- [6] W. Cheng, C.L. Fu, and Z. Qian, *A modified Tikhonov regularization method for a spherically symmetric three-dimensional inverse heat conduction problem*, Mathematics and Computers in Simulation 75 (2007), pp. 97–112.
- [7] J.V. Beck, B. Blackwell, and C.R. Saint-Clair *Inverse Heat Conduction: Ill Posed Problems*, Wiley, New York, 1985.
- [8] S. Chantasiriwan, *An algorithm for solving multidimensional inverse heat conduction problem*, Int. J. Heat and Mass Transfer 44 (2001), pp. 3823 – 3832.
- [9] J. Zhou, Y. Zhang, J. Chen, and Z. Feng, *Inverse estimation of surface heating condition in a three-dimensional object using conjugate gradient method*, Int. J. Heat and Mass Transfer 53 (2010), pp. 2643 – 2654.
- [10] C.H. Huang and M.T. Chaing, *A three-dimensional inverse geometry problem in identifying irregular boundary configurations*, Int. J. Thermal Sci. 48 (2009), pp. 502 – 513.
- [11] W.L. Chen and Y.C. Yang, *Inverse problem of estimating the heat flux at the roller/workpiece interface during a rolling process*, App. Thermal Engineering 30 (2010), pp. 1247–1254.
- [12] Y. Yang and W. Chen, *A nonlinear inverse problem in estimating the heat flux of the disc in a disc brake system*, App. Thermal Engineering 3 (2011), pp. 2439–2448.
- [13] F. Volle, D. Maillet, M. Gradeck, A. Kouachi, and M. Lebouché, *Practical application of inverse heat conduction for wall condition estimation on a rotating cylinder*, Int. J. Heat and Mass Transfer 52 (2009), pp. 210 – 221.
- [14] F. Lefevre and C.L. Niliot, *The BEM for point heat source estimation: application to multiple static sources and moving sources*, Int. J. Therm. Sci. 41 (2002), pp. 536–545.
- [15] M. Lazard and P. Corvisier, *Modelling of a Tool during turning. Analytical prediction of the temperature and of the heat flux at the tool's tip*, App. Thermal Engineering 24 (2004), pp. 839–849.
- [16] J. Battaglia, O. Cois, L. Puigsegur, and A. Oustaloup, *Solving an inverse conduction problem using a non integer identified model*, Int. J. Heat and Mass Transfer 44 (2001), pp. 2671–2680.
- [17] M. Girault and D. Petit, *Identification method in non-linear heat conduction. Part 1: Modal reduction*, Int. J. Heat and Mass Transfer 48 (2005), pp. 105–118.
- [18] M. Girault, E. Videcoq, and D. Petit, *Estimation of time-varying heat sources through inversion of a low order model built with the Modal Identification Method from in-situ temperature measurements*, Int. J. Heat and Mass Transfer 53 (2010), pp. 206 – 219.
- [19] H.M. Park and W.S. Jung, *Recursive Solution of an Inverse Heat Transfer Problem in Rapid Thermal Processing Systems*, Int. J. Heat and Mass Transfer 44 (2001), pp. 2053–2065.
- [20] O. Quéméner, J.L. Battaglia, and A. Neveu, *Résolution d'un problème inverse par utilisation d'un modèle réduit modal. Application au frottement d'un pion sur un disque en rotation*, Int. J. Thermal Sci. 42 (2003), pp. 361–378.
- [21] E. Videcoq, O. Quéméner, W. Nehme, and A. Neveu, *Real time heat sources identification by a branch eigenmodes reduced model*, in *ICIPE*, Paris Dourdan, 2008.
- [22] E. Videcoq, O. Quéméner, M. Lazard, and A. Neveu, *Heat Source Identification and On-Line Temperature Control by a Branch Eigenmodes Reduced Model*, Int. J. Heat and Mass Transfer 51 (2008), pp. 4743–4752.

- [23] E. Videcoq, M. Lazard, O. Quéméner, and A. Neveu, *Online Temperature prediction using a Branch eigenmode reduced model applied to cutting process*, Num Heat Transfer A 55 (2009), pp. 683–705.
- [24] O. Quéméner, F. Joly, and A. Neveu, *On-line heat flux identification from a rotating disk at variable speed*, Int. J. Heat and Mass Transfer 53, Issues 7-8 (2009), pp. 1529–1541.
- [25] C. Wagner, *Heat transfer from a rotating disk in ambient air*, J. of Appl. Phys 19 (1948), pp. 937–841.
- [26] E. Cobb and O. Saunders, *Heat transfert from a rotating disk*, Proc. Roy. Soc. A., Proc. Roy. Soc. ., A., 220 (1956), pp. 343–351.
- [27] S. aus der Wiesche, *Heat transfer from a rotating disk in a parallel air crossflow*, Int. J. Thermal Sci. 46 (2007), pp. 745 – 754.
- [28] O. Quéméner, A. Neveu, and E. Videcoq, *A Specific Reduction Method for Branch Modal Formulation: Application to Highly Non Linear Configuration*, Int. J. Thermal Sci. 46 (2006), pp. 890–907.
- [29] A. Neveu, K.E. Khoury, and B. Flament, *Simulation de la conduction non linéaire en régime variable: Décomposition sur les modes de branches*, Int. J. Thermal Sci. 38 (1999), pp. 289–304.
- [30] F. Joly, O. Quéméner, and A. Neveu, *Modal Reduction of an Advection-Diffusion Model using a Branch Basis*, Num. Heat. Transfer B 53 (2008), pp. 466–485.
- [31] <http://www.caam.rice.edu/software/ARPACK/>.
- [32] O. Quéméner, F. Joly, and A. Neveu, *The generalized amalgam method for modal reduction*, Int. J. Heat and Mass Transfer 55, (2012), pp. 1197–1207.
- [33] A. Anderson and R.A.Knapp, *Hot spotting in automotive friction systems*, in *International Conference on Wear of Materials, Denver (USA)*, Vol. 2, 1989, pp. 673 – 680.
- [34] S. Panier, P. Dufrénot, J. Brunel, and D. Weichert, *Progressive waviness distorsion : a new approach of hot spotting in disc brake*, Journal of Thermal Stresses 28 (2005), pp. 47 – 62.
- [35] T. Kao, J. Richmond, and A. Douarre, *Brake disc hot spotting and thermal judder : an experimental and finite element study*, International Journal of Vehicle Design 23 (2000), pp. 276 – 296.
- [36] A. Luikov *Analytical Heat Diffusion Theory*, Academic Press, New York, 1968.
- [37] W. Osterle and I. Urban, *Third body formation on brake pads and rotors*, Tribology International 39 (2006), pp. 401–408.
- [38] G. Ingo, M. Uffizi, G. Falso, G. Bultrini, and G. Padeletti, *Thermal and microchemical investigation of automotive brake pad wear residues*, Thermochimica Acta 418 (2004), pp. 61–68.
- [39] D. Gultekin, M. Uysal, S. Aslan, M. Alaf, M. Guler, and H. Akbulut, *The effects of applied load on the coefficent of friction in Cu-MMC brake pad/Al-SiCp MMC brake disc system*, Wear 270 (2010), pp. 73–82.

Appendix A. Discrete amplitude equation

The variational formulation of Eqs. (8)-(9) reads

$$\begin{aligned}
 c \int_{\Omega} g \frac{\partial T}{\partial t} d\Omega &= -k \int_{\Omega} \vec{\nabla} g \cdot \vec{\nabla} T d\Omega - c\omega(t) \int_{\Omega} g \vec{U}_0 \cdot \vec{\nabla} T d\Omega \\
 &\quad - h(t) \left(a \int_{\Omega} g T d\Omega + \int_{\Gamma} g T d\Gamma \right) \\
 &\quad + h(t) \left(a \int_{\Omega} g T_f d\Omega + \int_{\Gamma} g T_f d\Gamma \right) \\
 &\quad + f_1(t) \int_{\Omega} g \pi(M) d\Omega + f_2(t) \int_{\Gamma} g \varphi(M) d\Gamma,
 \end{aligned} \tag{A1}$$

where g is a trial function defined in $H^1(\Omega)$.

In Eq.(A1), the temperature field is replaced by its modal decomposition (Eq.(10)), while the test functions f are the adjoint branch problem eigenmodes. The amplitude equation reads then as :

$$\begin{aligned}
 c \sum_{i=0}^{\tilde{N}} \int_{\Omega} \tilde{V}_j^{*,t} \tilde{V}_i d\Omega \frac{\partial \tilde{x}_i}{\partial t} &= -k \sum_{i=0}^{\tilde{N}} \int_{\Omega} \vec{\nabla} \tilde{V}_j^{*,t} \cdot \vec{\nabla} \tilde{V}_i d\Omega \tilde{x}_i - c\omega(t) \sum_{i=0}^{\tilde{N}} \int_{\Omega} \tilde{V}_j^{*,t} \vec{U}_0 \cdot \vec{\nabla} \tilde{V}_i d\Omega \tilde{x}_i \\
 &\quad - h(t) \left(a \sum_{i=0}^{\tilde{N}} \int_{\Omega} \tilde{V}_j^{*,t} \tilde{V}_i d\Omega \tilde{x}_i + \sum_{i=0}^{\tilde{N}} \int_{\Gamma} \tilde{V}_j^{*,t} \tilde{V}_i d\Gamma \tilde{x}_i \right) \\
 &\quad + h(t) \left(a \int_{\Omega} \tilde{V}_j^{*,t} T_f d\Omega + \int_{\Gamma} \tilde{V}_j^{*,t} T_f d\Gamma \right) \\
 &\quad + f_1(t) \int_{\Omega} \tilde{V}_j^{*,t} \pi(M) d\Omega + f_2(t) \int_{\Gamma} \tilde{V}_j^{*,t} \varphi(M) d\Gamma,
 \end{aligned} \tag{A2}$$

where $\tilde{V}_j^{*,t}$ is the transpose of \tilde{V}_j^* . This is the reduced model state equation whose unknowns are \tilde{x}_i , and whose order is \tilde{N} . The following operators are defined :

$$\begin{aligned}
 \mathbf{K} &= k \int_{\Omega} \vec{\nabla} \bullet \cdot \vec{\nabla} g d\Omega & \mathbf{C} &= c \int_{\Omega} g d\Omega \\
 \mathbf{U} &= c \int_{\Omega} g \vec{U}_0 \cdot \vec{\nabla} \bullet d\Omega & \mathbf{H} &= a \int_{\Omega} g \bullet d\Omega + \int_{\Gamma} g \bullet d\Gamma \\
 \mathbf{T}_f &= a \int_{\Omega} g T_f d\Omega + \int_{\Gamma} g T_f d\Gamma & \mathbf{P} &= \int_{\Omega} g \pi(M) d\Omega \\
 \mathbf{F} &= \int_{\Gamma} g \varphi(M) d\Gamma
 \end{aligned} \tag{A3}$$

They are discretized on finite elements mesh with linear shape functions, leading to a mesh with N_{mesh} nodes. Noting $\tilde{\mathbf{V}}[N_{mesh} \times \tilde{N}]$ the matrix defining the reduced base, and $\tilde{\mathbf{V}}^{*,T}$ the transpose of the adjoint matrix, the equation system to solve is :

$$\begin{aligned} \tilde{\mathbf{V}}^{*,T} \mathbf{C} \tilde{\mathbf{V}} \dot{\tilde{\mathbf{X}}}(t) = & \tilde{\mathbf{V}}^{*,T} [\mathbf{K} + \omega(t)\mathbf{U} + h(t)\mathbf{H}] \tilde{\mathbf{V}} \tilde{\mathbf{X}} \\ & + h(t)\tilde{\mathbf{V}}^{*,T} \mathbf{T}_f + f_1(t)\tilde{\mathbf{V}}^{*,T} \mathbf{F} + f_2(t)\tilde{\mathbf{V}}^{*,T} \mathbf{P}. \end{aligned} \quad (\text{A4})$$

This equation can be rewritten as :

$$\mathbf{L} \frac{d\tilde{\mathbf{X}}}{dt} = [\mathbf{M}_K + \omega(t)\mathbf{M}_U + h(t)\mathbf{M}_H] \tilde{\mathbf{X}} + h(t)\mathbf{N}_{T_f} + f_1(t)\mathbf{N}_\pi + f_2(t)\mathbf{N}_\varphi, \quad (\text{A5})$$

Working in the amplitude space, and for a given number of modes \tilde{N} , matrices \mathbf{L} , \mathbf{M}_K , \mathbf{M}_U and \mathbf{M}_H , of dimension $[\tilde{N} \times \tilde{N}]$, are respectively the projection of inertia, conductance, transport and convective exchange matrices in the amplitude space, $\tilde{\mathbf{X}}$ is the amplitudes vector. The vectors \mathbf{N}_{T_f} , \mathbf{N}_π and \mathbf{N}_φ are respectively the ambient, volume and superficial solicitations vectors of dimension \tilde{N} . They are defined by Eq. (A4) according to their apparition order. The resulting linear system is of small size, but the matrices are full. For direct resolution the time discretization is done by a backward Euler scheme. The resulting linear system is solved by a LU method.

Appendix B. Beck Method adapted to reduced modal problem

Resolution of an inverse problem is done from temperature value on n particular points in the domain, named outputs, yielding a vector \mathbf{Y} of dimension n linked to the temperature field, and thus to the reduced modal base, by the following relations:

$$\mathbf{Y}(t) = \mathbf{S}T(t) = \mathbf{S}\tilde{\mathbf{V}}X(t) = \mathbf{H}\tilde{\mathbf{X}}(t) \quad (\text{B1})$$

A Beck sequential technique [7] with a constant time steps semi implicit temporal discretization is used. Indeed, time dependent parameters should not appear in the matrix that will be inversed. They are estimated at time step k :

$$\begin{aligned} \tilde{\mathbf{X}}(k+1) = & (\mathbf{L} - \delta t \mathbf{M}_K)^{-1} [\mathbf{L} + \delta t(\omega(k)\mathbf{M}_U + h(k)\mathbf{M}_H)] \tilde{\mathbf{X}}(k) \\ & + h(k+1)\delta t (\mathbf{L} - \delta t \mathbf{M}_K)^{-1} \mathbf{N}_{T_f} \\ & + f(k+1)\delta t (\mathbf{L} - \delta t \mathbf{M}_K)^{-1} \mathbf{N}_\pi \end{aligned} \quad (\text{B2})$$

The outputs vector expresses from Eqs. (B1) and (B2)

$$\begin{aligned} \mathbf{Y}(k+1) = & \mathcal{M}\mathbf{H} [\mathbf{L} + \omega(k)\delta t \mathbf{M}_U + h(k)\delta t \mathbf{M}_H] \tilde{\mathbf{X}}(k) \\ & + h(k+1)\delta t \mathcal{M}\mathbf{H}\mathbf{N}_{T_f} \\ & + f(k+1)\delta t \mathcal{M}\mathbf{H}\mathbf{N}_\pi, \end{aligned} \quad (\text{B3})$$

Or

$$\mathbf{Y}(k+1) = f(k+1)\mathbf{H}\mathcal{P} + \mathbf{H} \left[\mathcal{G}(k)\tilde{\mathbf{X}}(k) + h(k+1)\mathcal{F} \right], \quad (\text{B4})$$

with the following matrices

$$\begin{cases} \mathcal{M} = (\mathbf{L} - \delta t \mathbf{M}_K)^{-1} \\ \mathcal{G}(k) = \mathcal{M} [\mathbf{L} + \omega(k)\delta t \mathbf{M}_U + h(k)\delta t \mathbf{M}_H] \\ \mathcal{F} = \delta t \mathcal{M}\mathbf{N}_{T_f} \\ \mathcal{P} = \delta t \mathcal{M}\mathbf{N}_\pi \end{cases} \quad (\text{B5})$$

In order to take into account the lagging and damping effects of the diffusion process, it is necessary to obtain information using future time steps. A function specification is introduced. A temporary assumption is made on the additional unknowns: $f(k+1+1), \dots, f(k+1+nf)$, where nf is the number of future time steps. In this study, a constant value of f is chosen:

$$f(k+1+i) = f(k+1) = \text{constant for } 1 \leq i \leq nf \quad (\text{B6})$$

The addition of future time steps leads to the resolution of a system of $(nf+1) \times q$ equations where q is the number of measurements.

Hence, at each time step, the temperature measurements vector \mathbf{Y}^* contains $(nf+1) \times n$ rows, as follows:

$$\mathbf{Y}^* = \begin{bmatrix} \mathbf{Y}^*(k+1) \\ \mathbf{Y}^*(k+2) \\ \vdots \\ \mathbf{Y}^*(k+1+nf) \end{bmatrix} \quad (\text{B7})$$

The system to solve is then overdetermined. The aim is to identify the pseudo-solution $\hat{f}(k+1)$ source of the inverse heat advection-conduction problem, such as $\mathbf{Y}^* - \tilde{\mathbf{Y}} \cong 0$, where $\tilde{\mathbf{Y}}$ is the temperature vector computed by the reduced model. This condition can be written, according to Eq.

$$\mathbf{Y}^* - \left(\mathbf{C}\hat{f}(k+1) + \mathbf{D} \right) \cong 0 \quad (\text{B8})$$

with the following matrices

$$\mathbf{C} = \begin{bmatrix} \mathbf{H}\mathcal{P} \\ \mathbf{H}[\mathcal{P} + \mathcal{P}\mathcal{G}(k+1)] \\ \vdots \\ \mathbf{H} \left[\mathbf{I} + \sum_{j=1}^{nf} \prod_{i=j}^{nf} \mathcal{G}(k+i) \right] \mathcal{P} \quad \forall nf \geq 1 \end{bmatrix} \quad (\text{B9})$$

$$\mathbf{D} = \begin{bmatrix} \mathbf{H} \left[\mathcal{G}(k)\tilde{X}(k) + h(k+1)\mathcal{F} \right] \\ \mathbf{H} \left[\mathcal{G}(k)\mathcal{G}(k+1)\tilde{X}(k) + h(k+2)\mathcal{F} + h(k+1)\mathcal{G}(k+1)\mathcal{F} \right] \\ \vdots \\ \mathbf{H} \left[\prod_{i=0}^{nf} \mathcal{G}(k+i)\tilde{X}(k) + \right. \\ \left. \left[h(k+nf+1) + \sum_{j=1}^{nf} h(k+j) \prod_{i=j}^{nf} \mathcal{G}(k+i) \right] \mathcal{F} \right] \quad \forall nf \geq 1 \end{bmatrix} \quad (\text{B10})$$

The inversion procedure leads to the sequential solution :

$$\hat{f}(k+1) = (\mathbf{C}^T \mathbf{C})^{-1} \mathbf{C}^T (\mathbf{Y}^* - \mathbf{D}) \quad (\text{B11})$$

With the reduced model, matrix $(\mathbf{L} - \delta t \mathbf{M}_K)$ can be easily inverted, and thus the inverse problem can be solved, while it is impossible with the finite elements formulation due to the size of the matrix.

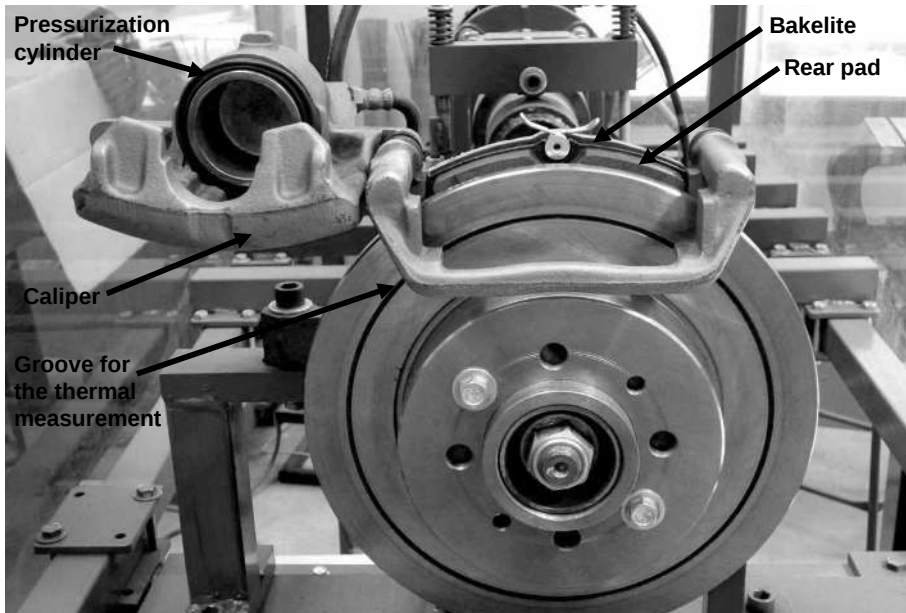


Figure 1. Experimental apparatus : the disc and the calliper (which is open) without the front pad

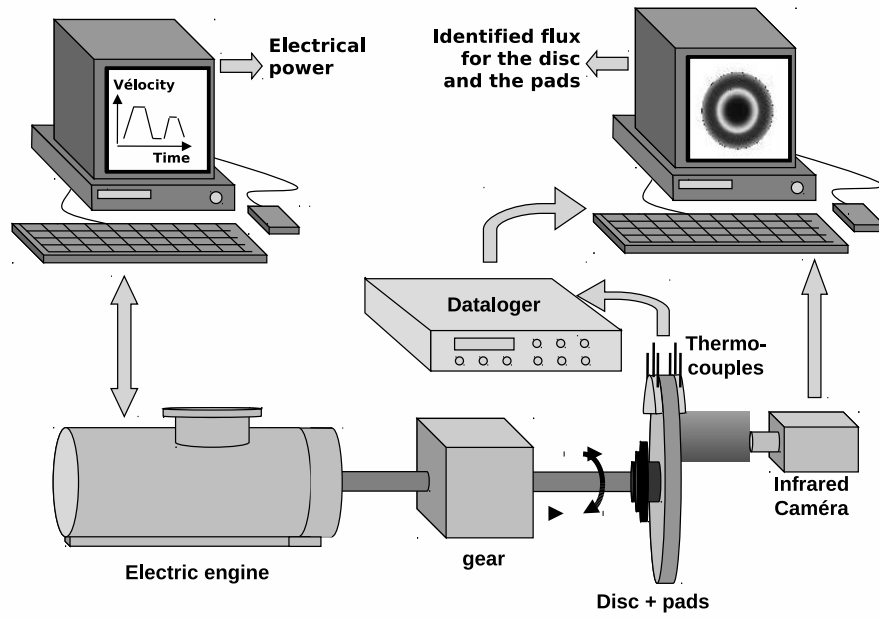


Figure 2. Principle of the test bench

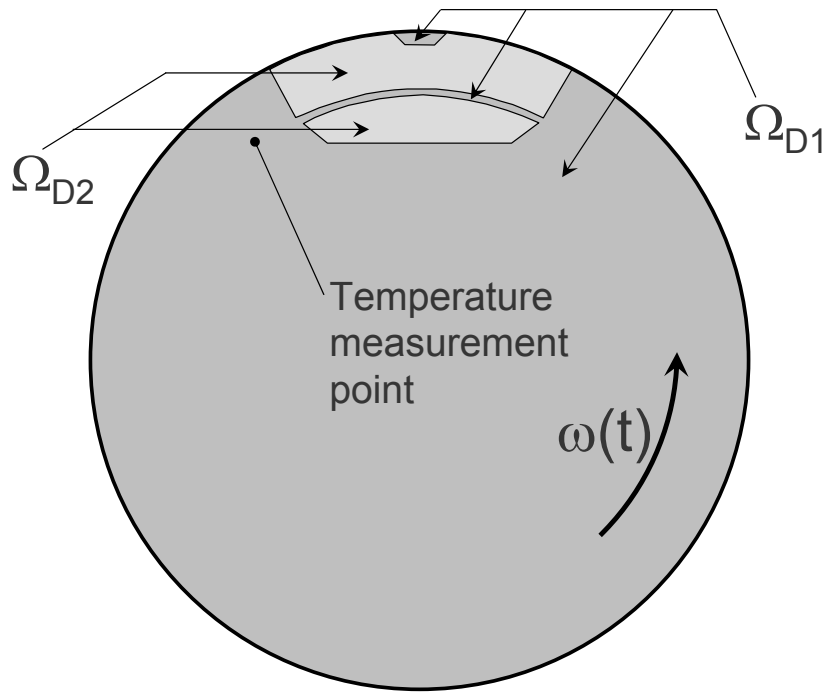


Figure 3. Disc geometry and location of the temperature measurement point

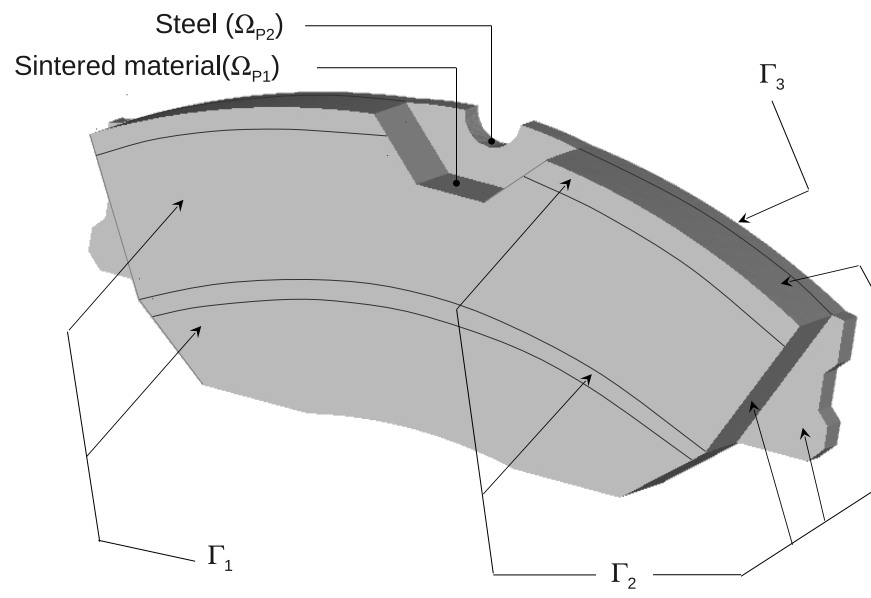


Figure 4. Pad geometry

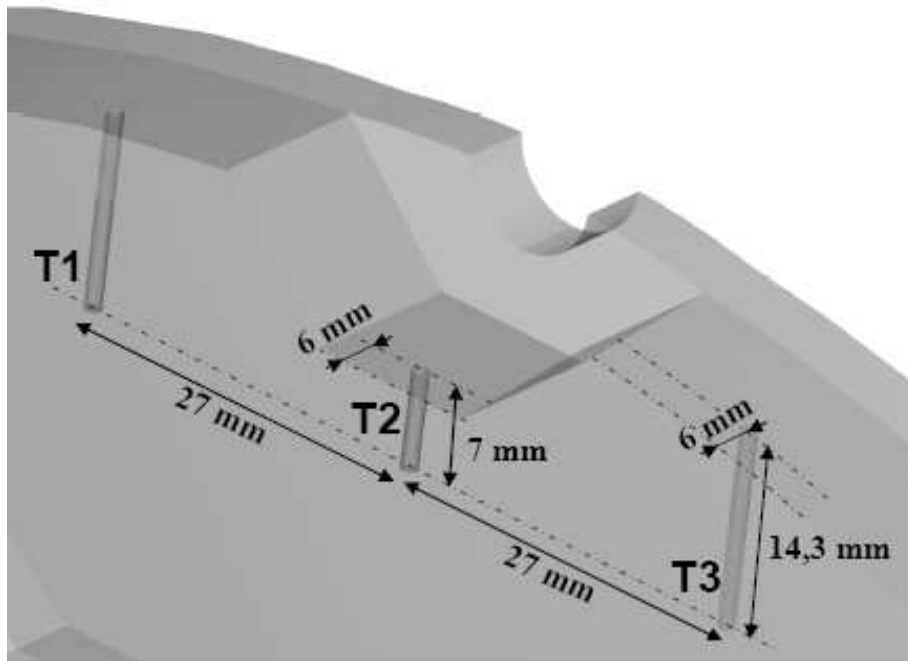


Figure 5. Location of the sensors in the pad

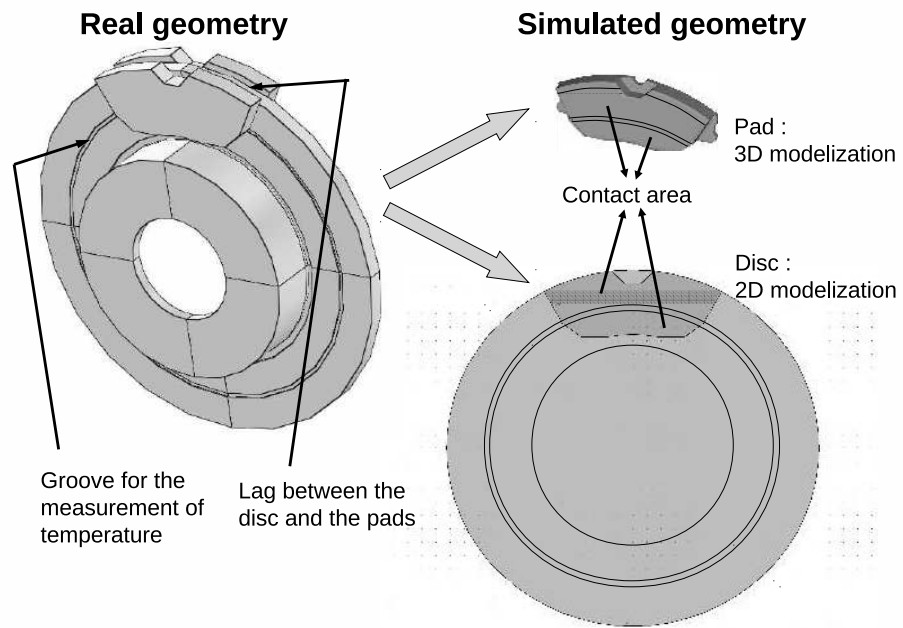


Figure 6. Modelization of the experiment

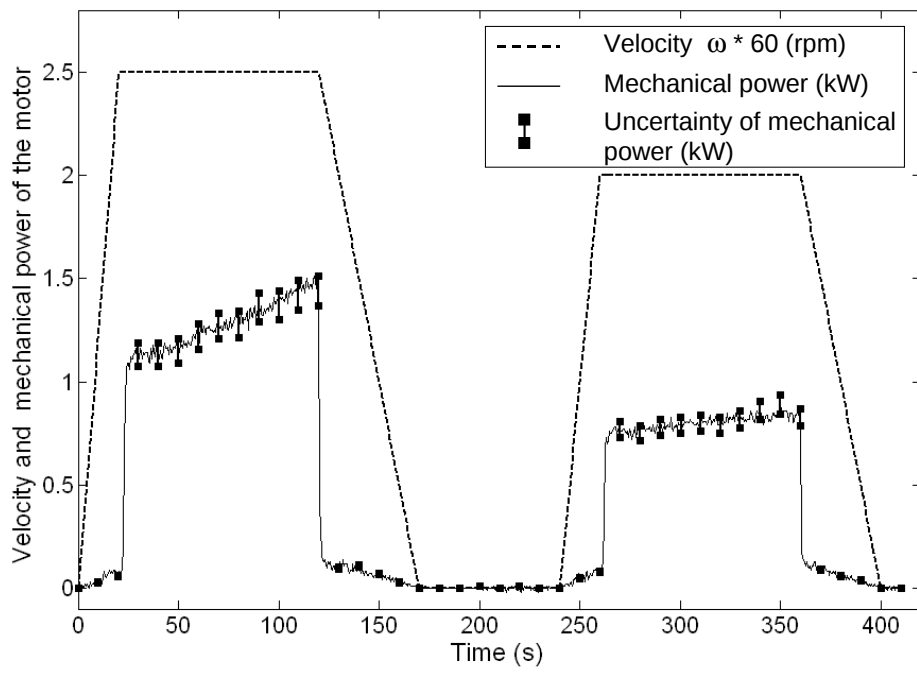


Figure 7. Mechanical measurements from the motor

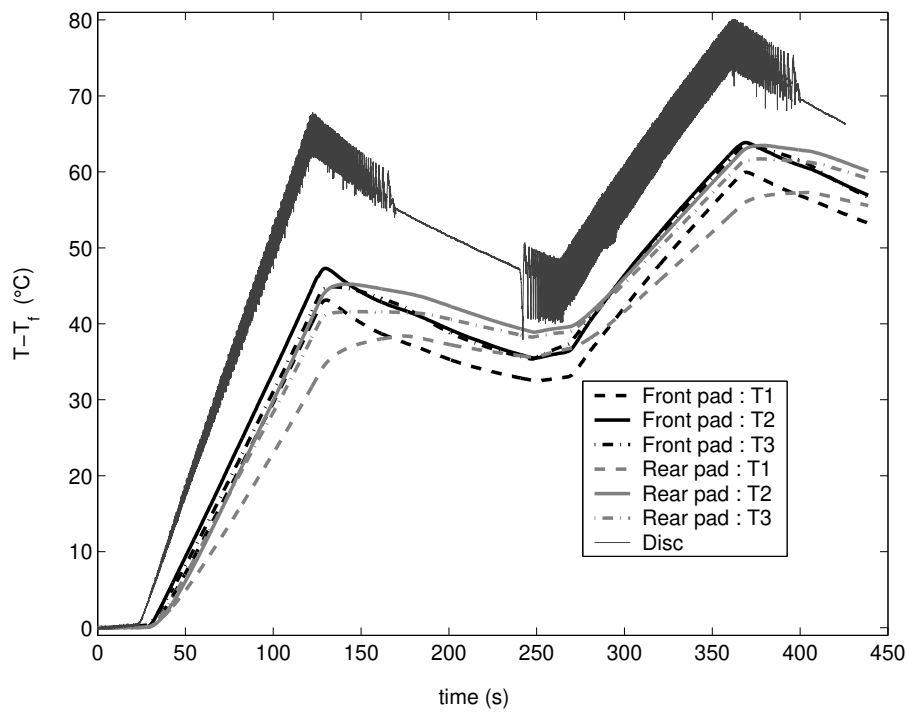


Figure 8. Temperature measurements

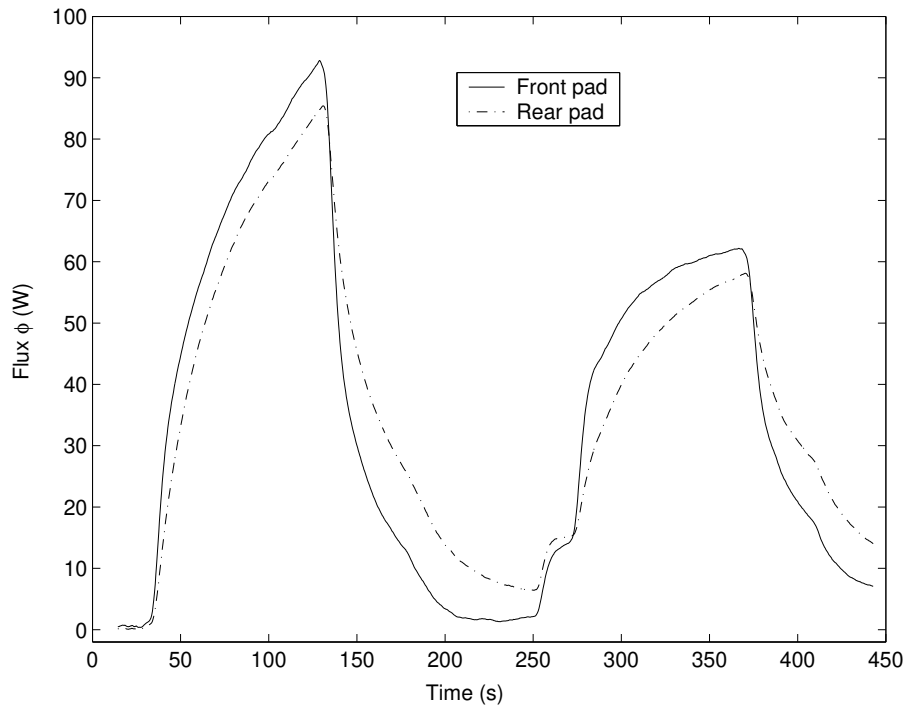


Figure 9. Identified heat flux received by the pads

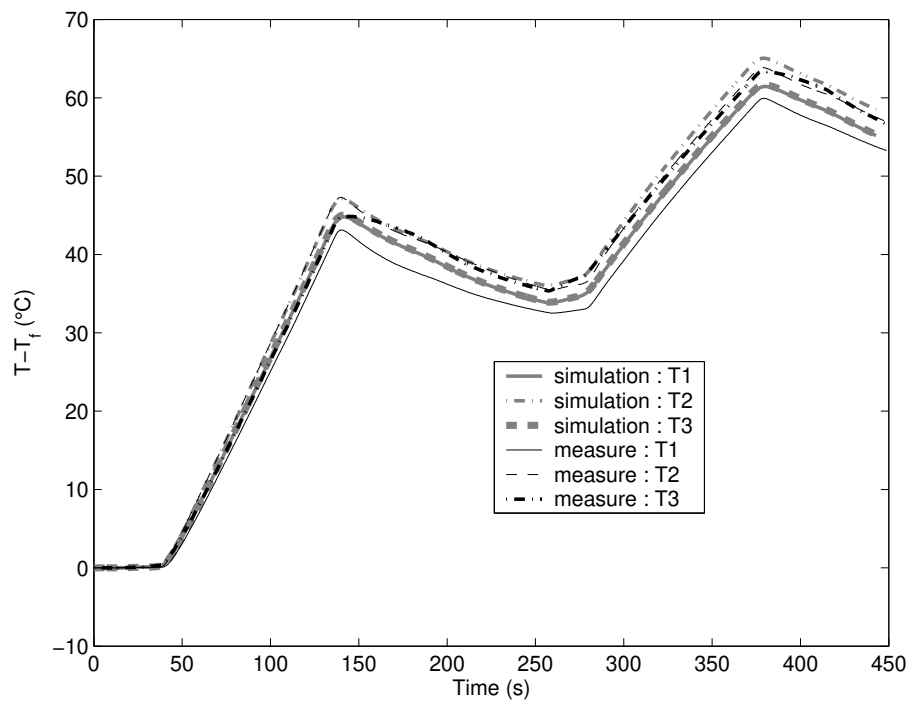


Figure 10. Front pad : comparison between measured and computed temperatures

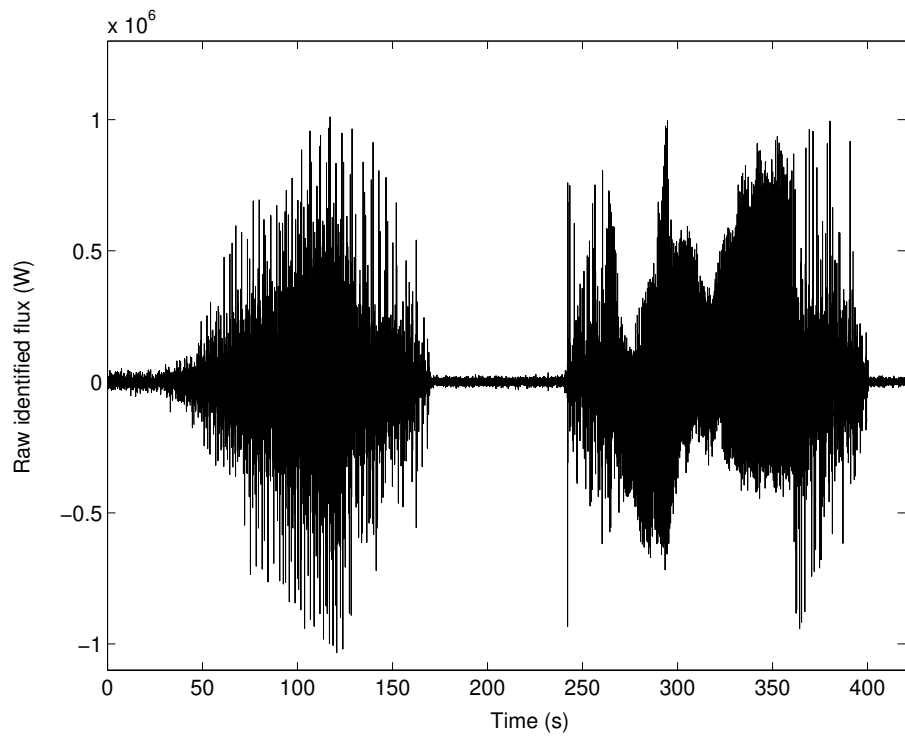


Figure 11. Identified heat flux received by the disc : raw result

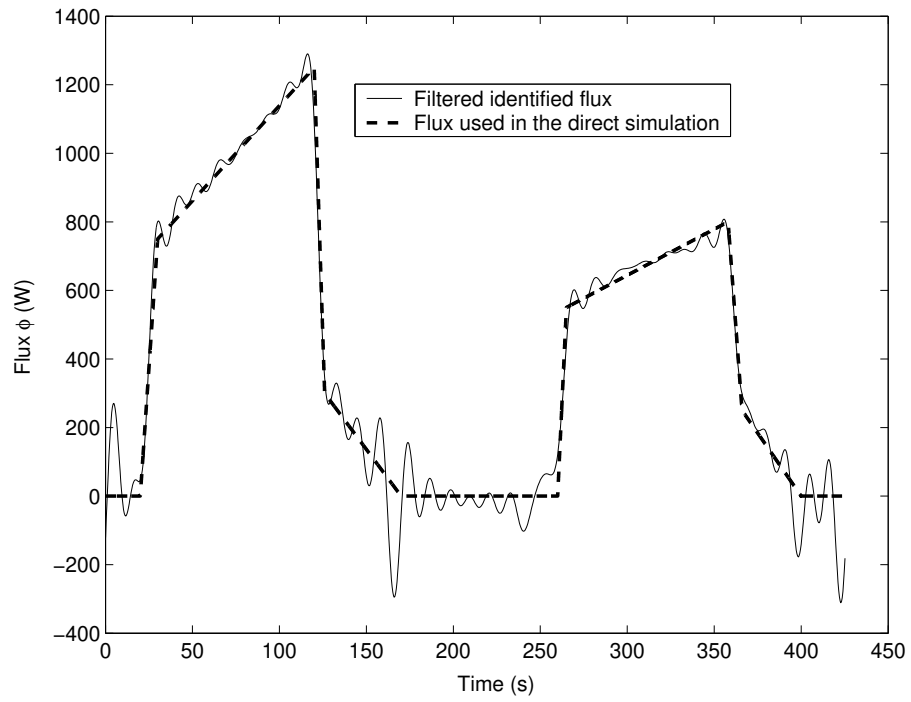


Figure 12. Filtered identified heat flux received by the disc and heat flux used in the direct simulation

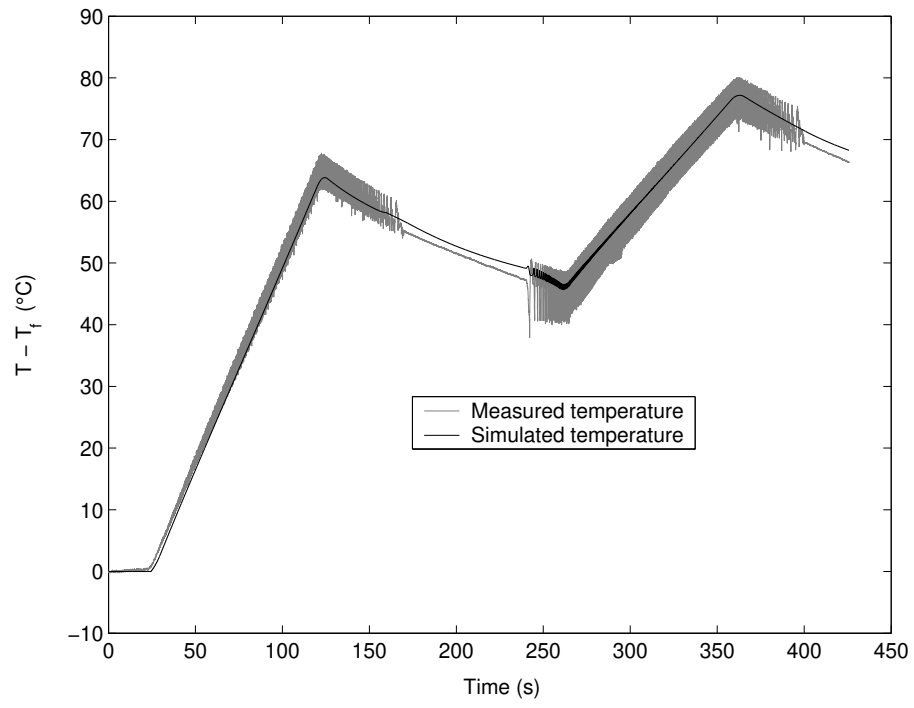


Figure 13. Disc : comparison between measured and computed temperatures

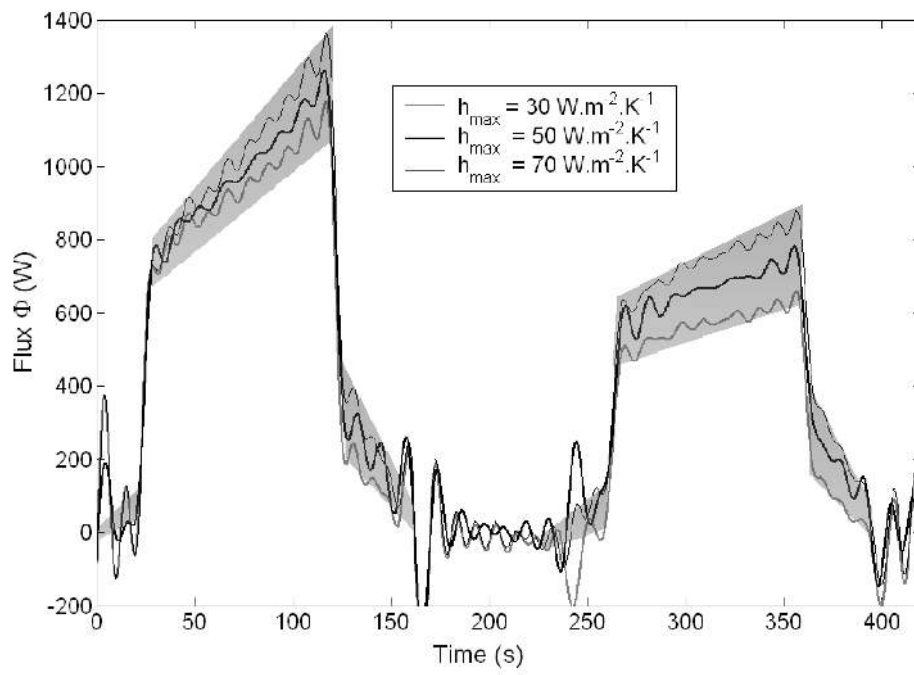


Figure 14. Influence of the exchange coefficient value on the filtered heat flux identification for the disc

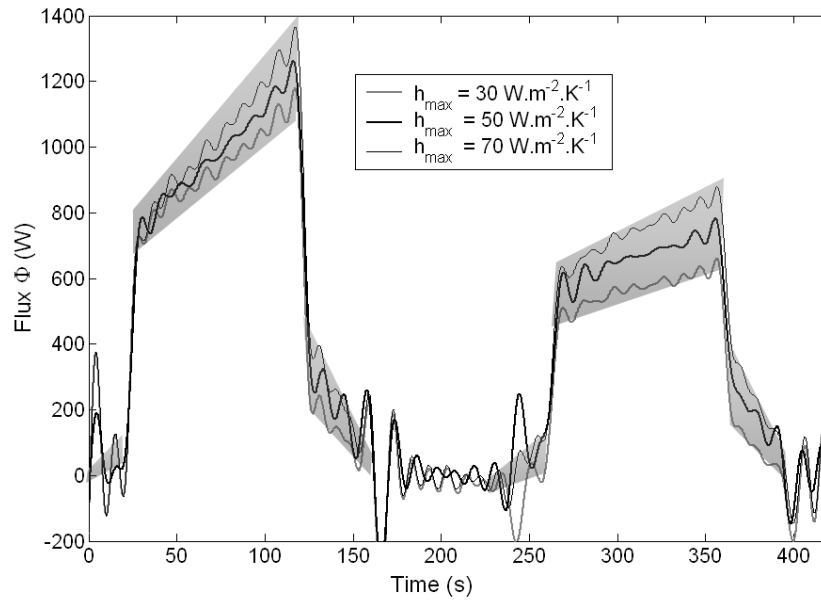


Figure 15. Influence of the exchange coefficient value on the filtered heat flux identification for the disc

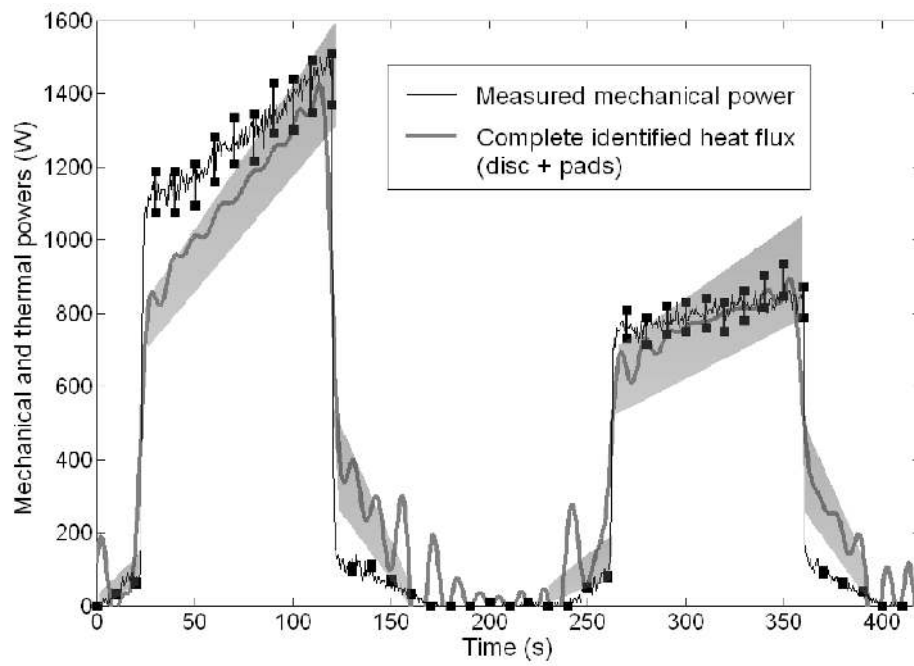


Figure 16. Comparison between the mechanical and the thermal powers

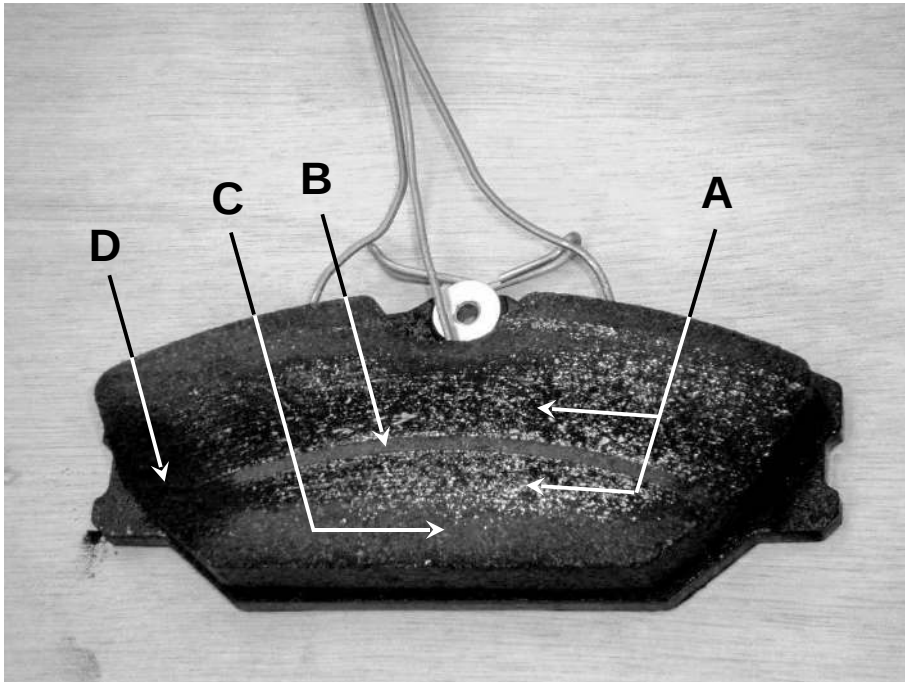


Figure 17. The pad after friction